Density functional theory study of dopants in polycrystalline TiO_2

Wolfgang Körner* and Christian Elsässer
Fraunhofer Institute for Mechanics of Materials IWM, Wöhlerstraße 11, F-79108 Freiburg, Germany
(Received 23 February 2011; revised manuscript received 8 April 2011; published 24 May 2011)

We present a density functional theory (DFT) study of doped rutile and anatase TiO_2 in which we investigate the impact of grain boundaries on the physics of atomic defects. The main goal is to obtain information about the positions of the defect levels generated by an oxygen vacancy, a titanium interstitial, cation dopants Nb, Al, and Ga, and an anion dopant N in the electronic band gap having in mind the application of TiO_2 as a transparent conducting oxide (TCO) or its use in heterogeneous catalysis. Due to the known deficiency of the local density approximation (LDA) of DFT to yield accurate values for band gap energies for insulators such as TiO_2, a self-interaction correction (SIC) to the LDA is employed. The main result of our study is that grain boundaries do affect the defect formation energies as well as the position and shape of the dopant-induced electronic energy levels significantly with respect to the single crystal. According to our study Nb doping may lead to *n*-conducting TiO_2 whereas doping with N, Al, or Ga is not promising in order to achieve *p*-conducting TiO_2. Furthermore an increase in the photoconductivity of TiO_2:N and the colorlessness of TiO_2:Al may be explained by our results.

DOI: 10.1103/PhysRevB.83.205315 PACS number(s): 61.72.Bb, 61.72.Mm

I. INTRODUCTION

Titanium dioxide has attracted an increasing amount of attention in recent years due to its numerous technological applications. TiO_2 is inexpensive and nontoxic, has a high oxidative power, and due its electronic band gap of 3.0 eV (rutile)[1,2] to 3.2 eV (anatase),[3] can serve as base material for transparent conducting oxide (TCO) thin-film systems that are getting widely used as electrodes in photovoltaic and optoelectronic technologies. Another large application field for TiO_2 is photocatalysis, which allows for example the selective destruction of highly toxic molecules. For the optimization of the functionality of the different TiO_2 devices a profound understanding of the defect physics is indispensable. In order to have good TCO properties, namely high electrical conduction and high optical transmission in the visible spectral range, extrinsic dopants that generate shallow electronic defect levels close to the band edges (of order $k_BT = 25$ meV) are needed. If TiO_2 is used for photocatalytic devices, deeper levels in the band gap (of order tenths of eV) are desired since they allow a better absorption of the solar spectrum.[4]

Our set of dopant elements is mainly chosen with regard to TCO applications. N, Al, and Ga are candidates for *p* doping and Nb is a candidate for *n* doping, which have so far been investigated by density functional theory (DFT) only for the rutile and anatase single crystals.[5–8] As important intrinsic point defects we investigated the oxygen vacancy and the titanium interstitial which are both assumed to be but have not been definitely established as a key reason for the intrinsic *n* conductivity of TiO_2.[9] Also the already existing DFT studies on these intrinsic defects (in rutile[10–12] or in anatase[13]) dealt with single crystals of TiO_2 as basic supercell models. However, real TiO_2 materials are usually polycrystalline with varying grain sizes of 10–100 nm.[14,15] This implies that TiO_2 systems contain many grain boundaries (GBs) which can influence the point-defect physics. In our previous study of polycrystalline ZnO,[16] we showed how the vicinity of grain boundaries can substantially change the formation energies for certain point defects and modify the defect levels in the electronic band structure.

In order to come to a realistic and representative set of atomistic models for our study of doped polycrystalline TiO_2 we constructed three rutile GB supercells and three anatase GB supercells which have atomic structures that have been partially observed experimentally.[17–19] In order to suppress GB-GB interactions in supercells with three dimensional periodic boundary conditions a sufficient number of layers of bulk structure in between two adjacent GBs is needed. This requirement leads to big supercells and long computation times.

Furthermore the task of studying the defect levels of dopants at GBs by DFT is complicated by the fact that an extension of the local density approximation (LDA) [or the generalized gradient approximation (GGA) as well] is needed because in the case of semiconductors, namely TiO_2, LDA and GGA underestimate the band gap by about thirty to fifty percent.[10,11,13,20–24] From the work of Perdew and Zunger[25] on free atoms it is known that these insufficiencies originate from the unphysical self-interaction that is present in approximate LDA or GGA exchange-correlation functionals. Inspired by Vogel *et al.*,[26] we have adapted a self-interaction correction (SIC) scheme[16] in which the SIC is incorporated in norm-conserving pseudopotentials (PPs) that is computationally not more involved than LDA.

In order to deduce which point defects are preferred and where they will be incorporated into a polycrystal (in bulk region or at grain boundaries?) we first determined the defect formation and segregation energies of the above-mentioned dopants. For the preferred charge states of the point defects in the bulk single crystals and at the GBs of rutile and anatase we then calculated the density of states (DOS) with our SIC-LDA approach in order to obtain accurate information about the position of the additional electronic levels.

The paper is organized as follows: In Sec. II we give the computational details about the SIC-LDA calculations and the supercell models. The obtained results of the total-energy and

electronic structure calculations are presented in Sec. III. A summary in Sec. IV concludes the paper.

II. THEORETICAL APPROACH

A. Mixed-basis pseudopotential method

The total-energy and electronic-structure calculations in this work were carried out on the basis of DFT by means of the computational mixed-basis pseudopotential (MBPP) method.[27–30] We used the LDA for exchange correlation as parameterized by Perdew and Zunger.[25] For Ti, O, and the impurity elements (Nb, Al, Ga, and N), norm-conserving pseudopotentials[31] were used for the core-valence interactions. The valence Bloch states were represented by a mixed basis of plane waves and additional, nonoverlapping atom-centered p orbitals for O and N ($2p$ states) and d orbitals for Ti, Nb, and Ga ($3d$ or $4d$ states). A plane-wave cutoff energy of 20 Ry (1 Ry = 13.606 eV) was determined to be sufficient for getting well-converged results. For the k-point sampling of the Brillouin-zone integrals in the total-energy calculations the Monkhorst-Pack meshes and a Gaussian broadening of 0.2 eV were used.

B. Self-interaction corrected pseudopotentials

As mentioned in the introduction we have chosen an implementation of the SIC that does not increase considerably the computational effort as compared to the ordinary LDA and thus is applicable to large atomistic supercells with up to 120 atoms. We incorporated the SIC into pseudopotentials for the atoms involved. The SIC-LDA calculations for supercells are then performed as the LDA calculations with the SIC-LDA PP used instead of LDA PP. A detailed description of this approach has been given by Vogel *et al.*[26] Our implementation is explained in detail in Ref. 16. In the following we only present a short summary and recall the notation.

Our self-interaction corrected pseudopotential $V_l^{\mathrm{SIC}}(r)$ in Kleinman-Bylander-type form reads

$$V_l^{\mathrm{SIC}}(r) = V_l(r) - \alpha\left\langle \Psi_l^{pp}, \mathrm{w}_l[V_{\mathrm{H}}[n_l] + V_{\mathrm{xc}}[n_l]]\Psi_l^{pp}\right\rangle \Psi_l^{pp}(r), \tag{1}$$

where $V_l(r)$ is the norm-conserving ionic LDA PP for the valence electrons (constructed for instance in the scheme proposed by Vanderbilt;[31] the subscript l denotes the principal and angular-momentum quantum number of the respective highest valence orbital). V_H and V_{xc} are the electrostatic Hartree and LDA exchange correlation potentials that depend on the pseudodensity of electron orbital l which is given by $n_l(r) = p_l|\Psi_l^{pp}(r)|^2$ where p_l is the orbital occupation number and $\Psi_l^{pp}(r)$ the pseudo–wave function. $\langle\ldots,\ldots\rangle$ denotes the scalar product. Furthermore weight factors w_l are introduced which can take values in between 0 and 1. With all $w_l = 1$ for occupied electronic orbitals the correction scheme is called *atomic* SIC (ASIC) which is valid for isolated atoms. The weight factors allow one to turn on and off the SIC gradually. The advantage is that one can build PPs that are better adjusted to the local environment in a solid. In the ionic compound TiO_2 for example the $3d$ orbitals of Ti form the conduction band and are nearly unoccupied. We take this into account by setting $w_2 = 0$ which means we do not apply the SIC to the $3d$ orbitals of Ti. The factor α is an empirical parameter that can be interpreted as a measure of the deviation of the ASIC potential from the exact SIC potential of the solid (see Ref. 32 for a detailed discussion).

TABLE I. The weight factors w_l used in Eq. (1) for the rutile structures. For the $2p$ orbitals of O and N slightly different weight factors w_1 were chosen (rutile/anatase). The reason is explained in detail in Sec. III D.

Weight Factor	Ti	O	N	Nb	Al	Ga
w_0	0	1.0	1.0	0	0	0
w_1	0	0.9/0.8	0.9/0.8	0	0	0
w_2	0	0	0	0	0	1.0

One can see in Eq. (1) that the weight factors w_l and the parameter α could be merged. The advantage would be to have less parameters in the model. However, we prefer to keep the parameters separated as they can be connected to physical properties of the considered system. The values the parameters taken in our model of TiO_2 are listed in Table I and explained in detail in Secs. III D and III E.

C. Supercells for grain boundaries and single crystals

Inspired by Refs. 17–19, we selected a representative set of three rutile and three anatase GB supercells with distinct structural units at the boundary. These supercell models are specified in Table II in terms of their boundary plane, tilt axis, and CSL parameter[33] Σ, the numbers of atoms per supercell, and the GB energy obtained by SIC-LDA (and LDA) calculations. Due to the periodic boundary conditions every GB supercell contains two equivalent GBs. Thus we always substituted two equivalent host atoms per GB supercell, which resulted in doping concentrations of 2.8 at. % for the $GB1_r$ and $GB4_a$ supercells and 1.7 at. % for the other GB supercells. As bulk reference structure we used a tetragonal $2 \times 2 \times 3$ supercell of 72 atoms for rutile and $3 \times 3 \times 2$ supercell of 108 atoms for anatase where the substitution of one titanium or

TABLE II. Supercell models for grain boundaries in rutile and anatase TiO_2. In the text we abbreviate the grain boundaries by $GB1_r$, $GB2_r$, and so on. The subscripts r and a indicate whether it is a rutile or anatase grain boundary. The boundary energy determined with SIC-LDA is the energy needed to insert the grain boundary into the bulk single crystal (LDA values are given in parentheses). For $GB6_a$ it was not possible to determine the boundary energy with SIC-LDA (indicated by *.*) according to Eq. (3) because the massive superposition of levels in the band gap made the determination of the individual energy shifts impossible.

Grain Boundary Notation	Atoms per Supercell	GB Energy (J/m^2)
$GB1_r$:(100)[100] $\Sigma 1$	72	0.47 (0.47)
$GB2_r$:(210)[001] $\Sigma 5$	120	1.92 (1.92)
$GB3_r$:(310)[001] $\Sigma 5$	120	2.84 (2.37)
$GB4_a$:(100)[100] $\Sigma 1$	72	1.09 (0.64)
$GB5_a$:(021)[100] $\Sigma 5$	120	1.32 (0.89)
$GB6_a$:(031)[100] $\Sigma 5$	120	*.* (2.36)

oxygen atom corresponds to an impurity concentration of 1.4 at. % and 0.9 at. %, respectively.

The bulk crystal and GB supercell models were structurally relaxed by shifting the atoms according to the Broyden-Fletcher-Goldfarb-Shanno (BFGS) algorithm[34] until the residual forces on all atoms were less than 0.001 Ry/a.u. (1 a.u. = 0.529 Å).

D. Formation and segregation energies with SIC-LDA

For the calculation of the formation energies we applied the formalism which is extensively explained in a review by Van de Walle and Neugebauer.[35] We determine the defect formation energy at the grain boundary ($m = \mathrm{GB}$) or in the bulk ($m = \mathrm{bulk}$) supercell by

$$E_f^m(d,q) = E_{\mathrm{tot}}^m(d,q) - E_{\mathrm{tot}}^m(h,q=0) + \mu(h) - \mu(d) - q\,\mu_e, \quad (2)$$

where $E_{\mathrm{tot}}^m(d,q)$ is the total energy of the supercell containing the defect d ($d = \mathrm{N}$, Al, Ga, V_{O}(= oxygen vacancy) or Ti_i (= titanium interstitial) plus q excess electrons. $E_{\mathrm{tot}}^m(h,q=0)$ is the total energy of the uncharged GB or bulk supercell where the host atom h ($h = \mathrm{O}$ or Zn) is not substituted. $\mu(h)$ and $\mu(d)$ denote the chemical potentials of the host and dopant atoms. μ_e is the chemical potential of the electrons (the Fermi level) relative to the valence band maximum, ranging from 0 to 3.0 eV for rutile and from 0 to 3.22 eV for anatase in the energy gap between the valence and conduction band edges.

Since the absolute value of the defect-formation energy for a certain doping material strongly depends on the reference material[36] we have selected stable materials that are likely to appear in growth processes. As references that compete with the incorporation in the crystal we have chosen gaseous molecular O_2 for oxygen and N_2 for nitrogen. For the other doping materials we have taken oxidic solid-state compounds. As reference materials for the metals niobium, aluminum, and gallium we have chosen Nb_2O_5, Al_2O_3, and Ga_2O_3.

We first determined the total energy of the supercell containing the defect with LDA: $E_{\mathrm{tot}}^m(d,q)$[LDA]. However, since the LDA underestimates the band gap and the electronic defect levels above the valence-band maximum (VBM) are in general too low in energy this LDA total energy is too low if states above the VBM are occupied.[37,38] Therefore we add to $E_{\mathrm{tot}}^m(d,q)$[LDA] a correction

$$\Delta\epsilon_d = \left[\epsilon_d^{\mathrm{SIC}} - \epsilon_{\mathrm{VBM}}^{\mathrm{SIC}}\right] - \left[\epsilon_d^{\mathrm{LDA}} - \epsilon_{\mathrm{VBM}}^{\mathrm{LDA}}\right] \quad (3)$$

for every occupied defect level ϵ_d above the VBM. The first bracket is the energy of an electron relative to the VBM determined by the SIC-LDA calculation; the second bracket is the energy of an electron relative to the VBM determined by the LDA calculation. A discussion and justification of this correction is given in Ref. 37.

Based on total energies of different suitable supercells one can determine segregation energies of point defects. As in our previous paper[16] we determined the segregation energy E_{seg} by two methods. Method 1 applied for example by Carlson *et al.*[39] is to calculate the defect formation energy in the GB and in the corresponding bulk supercell of the same size. Then $E_{\mathrm{seg}} = E_f^{\mathrm{GB}}(d,q) - E_f^{\mathrm{bulk}}(d,q)$. Method 2 calculates the total energy of the GB supercell where the dopant sits in the bulk region as far as possible away from the grain boundaries which appear periodically. Such arranged supercells are depicted in Figs. 1, 2, and 3. The segregation energy is then the difference of the total energies of the supercells with the impurity at the boundary $E_{\mathrm{tot}}^{\mathrm{GB}}$ and in the bulk region $E_{\mathrm{tot}}^{\mathrm{BR}}$: $E_{\mathrm{seg}} = E_{\mathrm{tot}}^{\mathrm{GB}}(d,q) - E_{\mathrm{tot}}^{\mathrm{BR}}(d,q)$. Both formulas for E_{seg} are defined such that a negative sign of the segregation energy indicates the preference of the dopant to sit at the boundary.

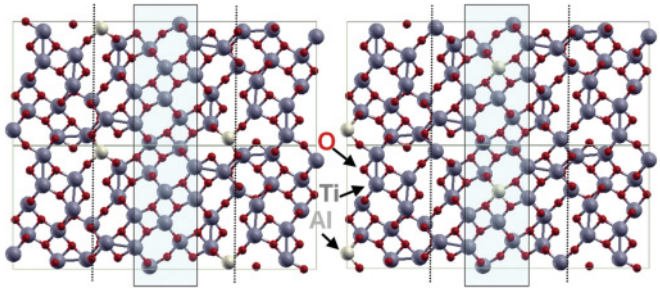

FIG. 1. (Color online) On the left: View from [100] on two supercells (120 atoms each) of the anatase $GB5_a$:(021)[100] Σ5 doped with Al substituting Ti at the GB. On the right: View from [100] on two relaxed supercells doped with Al substituting Ti in the bulk region. The dotted lines indicate the grain boundaries and the shaded area the bulk region. The special feature of $GB5_a$ is two oxygen atoms with dangling bonds per grain boundary unit cell. This feature explains the extraordinary behavior of this GB concerning preferred charge states as well as electronic defect levels (see Secs. III C and III E).

III. RESULTS AND DISCUSSION

A. TiO_2 single crystals

As a prerequisite for the study of dopants and interfaces, the structural parameters of the rutile and anatase TiO_2 single crystals were determined by DFT calculations with the MBPP

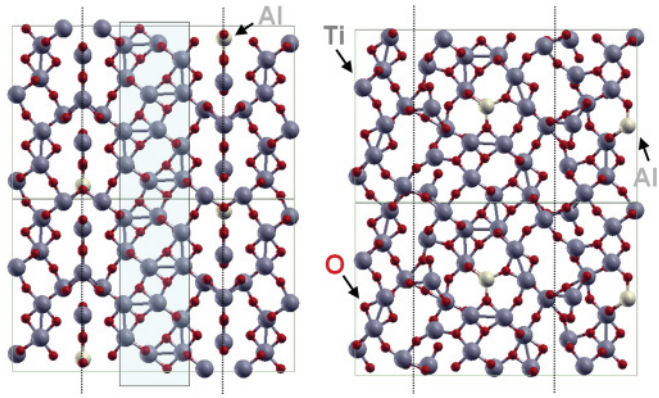

FIG. 2. (Color online) On the left: View from [100] on two supercells of the anatase $GB6_a$:(031)[100] Σ5 doped with Al substituting Ti at the GB. On the right: View from [100] on two supercells of the $GB6_a$:(031)[100] Σ5 where Ti atoms were substituted by Al atoms in the bulk region. The dotted lines indicate the grain boundaries and the shaded area the bulk region. The relaxation strongly disturbed the anatase bulk region because the bulk structure did not have a sufficient width.

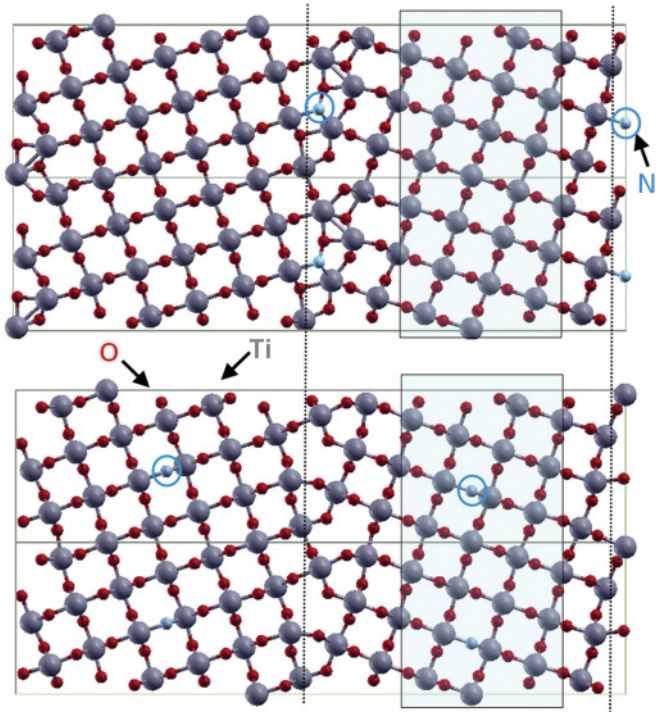

FIG. 3. (Color online) View from [001] on four supercells (120 atoms each) of the rutile GB2$_r$:(210)[001] Σ5 doped with N substituting O at the GB (top) and in the bulk region (bottom). The dotted lines indicate the grain boundaries and the shaded area the bulk region. In the bulk region N stays at the substitutional O site surrounded by three Ti atoms whereas at the GB it forms a N-O unit.

code and LDA-PP. The obtained values given in Table III deviate about one percent from the experimental values for rutile and anatase,[40] which are typical deviations for LDA results.

B. TiO_2 grain boundaries

The three rutile and three anatase GB models studied in this work are listed in Table II. From the differences of total energies of the undoped GB supercells and the corresponding bulk supercells we determined the GB energies given in the last column of Table II. The GB1$_r$ is only a weak disturbance of the perfect rutile structure which is reflected in its low energy of only 0.47 J/m^2. The corresponding anatase Σ1 grain boundary GB4$_a$, which also has a low energy, differs more from the anatase bulk reference structure. Some oxygen atoms at the boundary have only 2 instead of 3 Ti neighbors (=oxygen dangling bonds). In GB1$_r$ all oxygen atoms have coordinations like in the rutile bulk structure. This decisive structural difference will be important for the understanding of the different segregation behavior of extrinsic dopants in Sec. III C as well as for the understanding of the electronic structure in Sec. III E.

All the other GBs, some of which are shown in Figs. 1, 2, and 3, deviate more from the rutile or anatase perfect crystal and thus require more energy to be formed (for GB2$_r$ Dawson *et al.*[22] reported a boundary energy of 1.72 J/m^2 which is close to our 1.92 J/m^2). Just as GB4$_a$, they all have undercoordinated oxygen atoms at the boundary plane. GB5$_a$ even has two oxygen dangling bonds per GB unit (see Fig. 1). The consequences of these structural differences will be discussed in Secs. III C and III E.

TABLE III. Table of structural parameters for rutile and anatase TiO_2. The u is the free parameter of the Wyckoff positions 4f or 8e for oxygen atoms in rutile or anatase, respectively.

Lattice Parameter	Rutile TiO_2	Anatase TiO_2
a (LDA)	4.575	3.80
a (Exp.)	4.594[a]	3.785[a]
c/a (LDA)	0.64	2.45
c/a (Exp.)	0.644[a]	2.514[a]
u (LDA)	0.3025	0.21
u (Exp.)	0.305[a]	0.208[a]

[a]Reference 40.

C. Formation and segregation energies

The formation energy of a point defect determines in which concentration it will appear in a material. In Table IV we give the formation energies determined with SIC-LDA (LDA value in parentheses) for the neutral point defects N_O, Nb_{Ti}, Al_{Ti}, and Ga_{Ti} for oxygen-rich conditions; i.e., at the oxygen chemical potential $\mu_O = 0$ eV. μ_O can vary in the interval $H_F[TiO_2] \leqslant \mu_O \leqslant 0$ where $H_F[TiO_2] = -9.74$ eV (taken from Cox *et al.*[41]) is the experimental enthalpy of formation of TiO_2. The formation energies of the different dopants for intermediate or Ti-rich conditions can be obtained with the formulas $E_f(N_O) + \mu_O$, $E_f(Nb_{Ti}) + 0.5\mu_O$, $E_f(Al_{Ti}) + 0.5\mu_O$, and $E_f(Ga_{Ti}) + 0.5\mu_O$.

Before discussing the details of the individual dopants we summarize three general trends:

(1) In most cases the formation energies of the considered point defects are lower at the GBs than in the bulk (see Table IV).

TABLE IV. Comparison of the defect formation energies (values in eV) of the dopants (charge state $q = 0$, oxygen-rich conditions) for the six different grain boundaries determined with SIC-LDA. The results of the LDA calculation [i.e., without the correction of Eq. (3)] are given in parentheses. For GB6$_a$ it was not possible to determine the defect formation energies with SIC-LDA (indicated by *.*) according to Eq. (3) because the massive superposition of levels in the band gap made the determination of the individual energy shifts impossible. Also the LDA values for GB6$_a$ which deviate strongly from the other systems have to be taken with caution since the bulk region for GB6$_a$ is small (see Fig. 2).

(eV)	N_O	Nb_{Ti}	Al_{Ti}	Ga_{Ti}
$E_f^{\mathrm{Bulk}_r}$	2.88 (2.63)	2.17 (0.67)	0.89 (0.89)	0.48 (0.48)
$E_f^{\mathrm{GB1}_r}$	2.75 (2.50)	2.60 (1.10)	1.20 (1.20)	0.96 (0.96)
$E_f^{\mathrm{GB2}_r}$	3.81 (2.16)	1.84 (0.49)	0.07 (0.07)	0.00 (0.00)
$E_f^{\mathrm{GB3}_r}$	1.42 (1.67)	1.07 (0.22)	−0.87 (0.43)	−1.50 (−0.25)
$E_f^{\mathrm{Bulk}_a}$	2.78 (2.78)	1.83 (0.68)	1.31 (1.31)	0.99 (0.99)
$E_f^{\mathrm{GB4}_a}$	−0.59 (1.21)	0.57 (1.47)	−1.11 (1.37)	−1.51 (1.03)
$E_f^{\mathrm{GB5}_a}$	0.29 (2.49)	2.43 (1.38)	−2.46 (0.54)	−2.76 (0.23)
$E_f^{\mathrm{GB6}_a}$	*.* (−0.19)	*.* (−2.10)	*.* (−0.62)	*.* (−1.79)

TABLE V. Segregation energies of the four considered dopants (values in eV) for five grain boundaries in rutile and anatase TiO_2 determined with SIC-LDA by method 1. (The results obtained by method 2 are given in parentheses.) For $GB6_a$ the segregation energies could not be determined because the bulk region was strongly disturbed after relaxing the supercell containing the extrinsic dopant (see Fig. 2).

GB	$E_{seg}(N_O)$	$E_{seg}(Nb_{Ti})$	$E_{seg}(Al_{Ti})$	$E_{seg}(Ga_{Ti})$
$GB1_r$	0.16	0.37	0.25	0.41
	(0.09)	(0.03)	(0.32)	(0.36)
$GB2_r$	1.30	−0.14	−0.80	−0.40
	(1.36)	(−0.40)	(−0.63)	(−0.45)
$GB3_r$	−1.20	−0.85	−1.68	−1.90
	(−0.92)	(−0.97)	(−1.44)	(−1.53)
$GB4_a$	−3.37	−1.41	−2.47	−2.55
	(−3.27)	(−1.50)	(−2.26)	(−2.32)
$GB5_a$	−2.49	0.51	−3.84	−3.84
	(−2.18)	(0.72)	(−3.42)	(−3.41)

(2) The formation energies at $GB1_r$ differ only very little from the bulk values due to the high structural similarity of $GB1_r$ to the bulk structure of rutile. The other GBs provide deviating local environments which allow often energetically favorable relaxations.

(3) A gain in energy at the GBs is also reflected in the negative segregation energies in Table V. However, the given values should be taken with caution since in order to obtain segregation energies for the dilute limit of dopants one should work with big enough supercells where the periodically appearing GBs+dopants are sufficiently separated (see discussion in Ref. 16). Unfortunately due to the time-consuming DFT calculations one is limited today to GB supercells of about 100 atoms which imply bulk regions between the adjacent GBs of only a few layers (see Figs. 1, 2, and 3). The bulk region of the supercell modeling $GB6_a$ was still too small to obtain the segregation energies at all. For method 2 one has to place a dopant atom in the middle of the bulk region and relax the supercell. On the left of Fig. 2 we show the relaxed case of Al. The few bulk layers are strongly disturbed and thus the segregation energy derived from such a supercell is meaningless. Fortunately we encountered such a problem only for $GB6_a$. Successful examples of doped relaxed structures are shown in Figs. 1 and 3 where the bulk regions are structurally intact.

Since point defects can exchange electrons with their environment one needs to investigate also charged defect states. As $GB1_r$ is very similar to the bulk and $GB6_a$ has limited predictive value due to its small bulk region, we determined the favorable charge states for the different dopants only at the four other GBs. Figure 4 shows the defect formation energies for both bulk structures, $GB2_r$, $GB3_r$, $GB4_a$, and $GB5_a$. The formation energies are given as functions of the chemical potential of the electrons μ_e which can vary in between 0 and 3.0 eV for rutile and from 0 and 3.22 eV for anatase. In order to put results for rutile and anatase structures in the same graph we have only drawn the range from 0 to 3 eV. Low values of μ_e correspond to the *p*-conducting regime whereas values close to 3 eV correspond to the *n*-conducting regime.

As reference for the extrinsic dopants we also calculated the two intrinsic defects V_O and Ti_i. Both are discussed as possible sources of the intrinsic *n* conductivity of TiO_2. Our findings agree with recent results[42,43] beyond LDA and will be published in a comparative study of TiO_2 with rutile or anatase structure.

1. *n-type dopant* Nb *in* TiO_2

According to Fig. 4 Nb is an effective donor (positive charge state). In the bulk structures as well as at $GB2_r$ and $GB4_a$ Nb defects prefer the Nb_{Ti}^{+} state which agrees with the

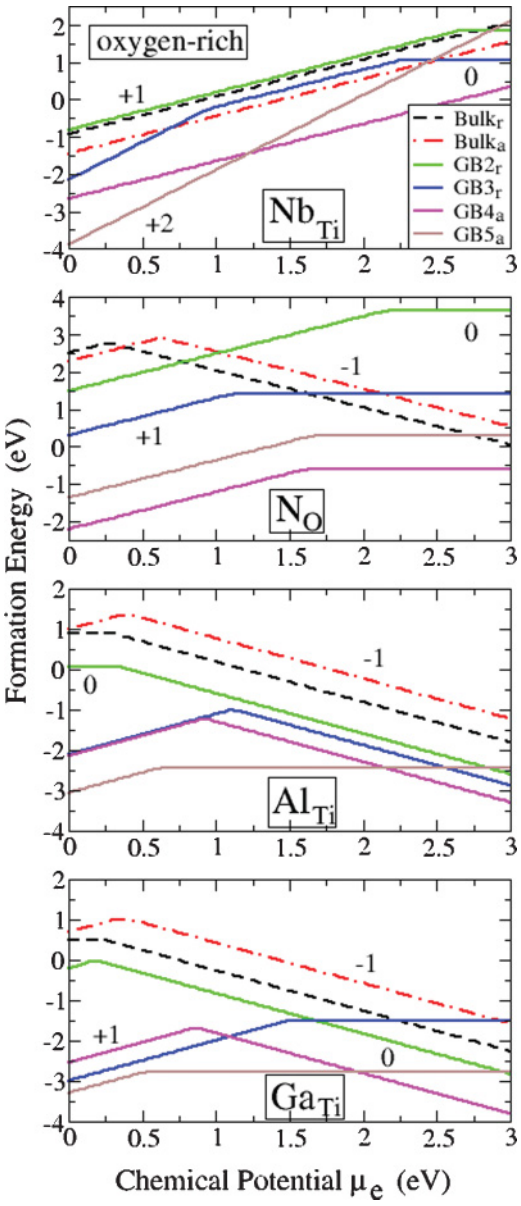

FIG. 4. (Color online) Defect formation energies for the dopants in the bulk and at four selected GBs as function of the chemical potential μ_e of the electrons under oxygen-rich conditions ($\mu_O = 0$). Values of μ_e close to 0 eV correspond to the *p*-conducting regime whereas values of μ_e close to 3.0 eV correspond to the *n*-conducting regime. The numbers +2, +1, 0, and −1 assign the preferred charge states.

results of Ref. 7 where TiO_2 in the bulk anatase structure was investigated. At $GB3_r$ the Nb_{Ti}^{2+} charge state is preferred for low values of μ_e which can be explained by an O atom that is only bound to the Nb dopant and thus has a strongly reducing influence. At $GB5_a$ the Nb_{Ti}^{2+} charge state is dominant for the whole range of μ_e. The reason is the presence of two under-coordinated oxygen atoms close to the Nb defect at $GB5_a$ which facilitate the donation of two electrons. Single under-coordinated oxygen atoms per boundary unit, like at $GB2_r$ and $GB4_a$, did not show similar effects (which was also seen in our ZnO study[16]). Apparently their attraction of electrons is too weak.

2. *p-type dopants* N, Al, *and* Ga *in* TiO_2

The three possible *p*-type dopants N, Al, and Ga show low formation energies over the whole range of μ_e. However in the decisive *p*-conducting regime they turn into donors (N_O^+, Al_{Ti}^+, and Ga_{Ti}^+). For TiO_2 in the bulk rutile structure Al and Ga defects adopt neutral states Al_{Ti}^0 and Ga_{Ti}^0 which are not counterproductive but also do not serve as acceptors. Thus our results would classify N, Al, and Ga as not promising dopants for the production of *p*-type TiO_2.

Concerning TiO_2:N the basic question of how N is incorporated is still under discussion (see Ref. 8 and references therein). In our considered structures N stayed at the substitutional sites for the bulk structures (and the bulklike $GB1_r$) whereas at the GBs a strong N-O bond was formed ($d_{N-O} = 1.38$–1.45 Å) during the relaxation of the structures (see Fig. 3), which is in line with Ref. 8, where the bond of interstitial nitrogen to oxygen ($d_{N-O} = 1.36$ Å) was found to be favorable.

The proximity of oxygen at the GBs does not allow the N_O defect to turn into a N_O^- defect (see Fig. 4).

In the presence of the electronegative unsaturated oxygen atoms provided at GBs the N_O, Al_{Ti}, and Ga_{Ti} defects cannot bind an extra electron (resulting in negative acceptor states) but even turn into donors for small values of μ_e as already mentioned.

In summary, strongly deviating local coordinations at the GBs can lead to changes of preferred defect states whereas minor deviations such as just one oxygen dangling bond near an extrinsic defect do not lead to a modified charge state compared to the bulk. Especially N has the tendency to form N-O units at GBs.

In the following we present the electronic-structure results for perfect bulk structures, undoped GBs, and finally point defects in the bulk or at GBs.

D. Bulk band structure of TiO_2: LDA vs SIC-LDA

In Fig. 5 our LDA result for the band structure of bulk TiO_2 in the rutile structure is shown. Each group of bands is labeled according to the dominant orbitals involved. The LDA band gap of only 1.55 eV is much smaller than the experimental gap of 3.0 eV.[1,2] Figure 6 shows our result with the SIC-LDA PP approach. For the orbitals of Ti atoms we did not apply the SIC. The outer 4*s*, 4*p*, and 3*d* orbitals are uncorrected because these are almost unoccupied in TiO_2. In the case of O we fully corrected the 2*s* orbitals ($w_0 = 1$) but only partially corrected the 2*p* orbitals ($w_1 = 0.9$). Combined with a value $\alpha = 0.8$ we obtained a very satisfying band gap value of 3.02 eV. The SIC O 2*p* valence band width of 6.11 eV (LDA 5.85 eV) is slightly bigger than the measured band width of 5.5 eV.[44] The fact that the LDA shows a better agreement concerning the band width is of minor relevance as for the defect levels the band gap is more important.

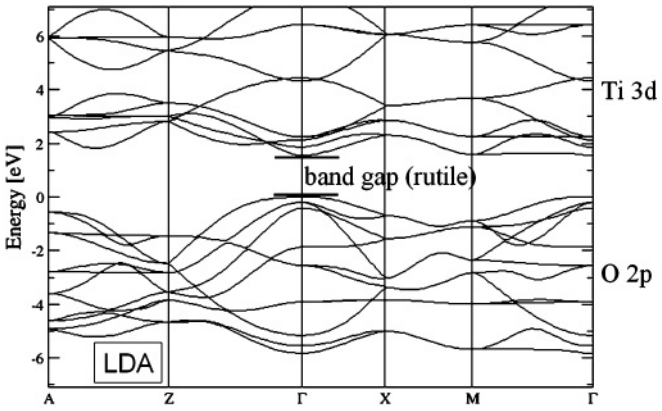

FIG. 5. Band structure of bulk TiO_2 (rutile structure) calculated in LDA. The VBM is set to 0 eV. We find a LDA band gap of 1.55 eV. The primary orbital character for each group of bands is indicated on the right side.

In Fig. 7 our LDA result for the band structure of bulk TiO_2 in the anatase structure is shown. The LDA band gap of only 1.73 eV is much smaller than the experimental gap of 3.2 eV.[3] Figure 8 shows our result with the SIC-LDA PP approach. Like for rutile we did not apply the SIC to the Ti atoms. In the case of O we fully corrected the 2*s* orbitals ($w_0 = 1$) but only partially corrected the 2*p* orbital ($w_1 = 0.8$) and kept a value of $\alpha = 0.8$. We obtained a satisfying band gap value of 3.22 eV. Our O 2*p* valence band width of 4.81 eV calculated with SIC (LDA 4.82 eV) almost agrees with the measured band width of 4.70 ± 0.05 eV.[45]

At a first glance it may appear desirable to treat TiO_2 in the rutile and anatase structure with the same SIC-PP for the O atom. With a *mean* value $w_1 = 0.85$ for the O 2*p* orbitals the rutile band gap was 2.81 eV and the anatase band gap

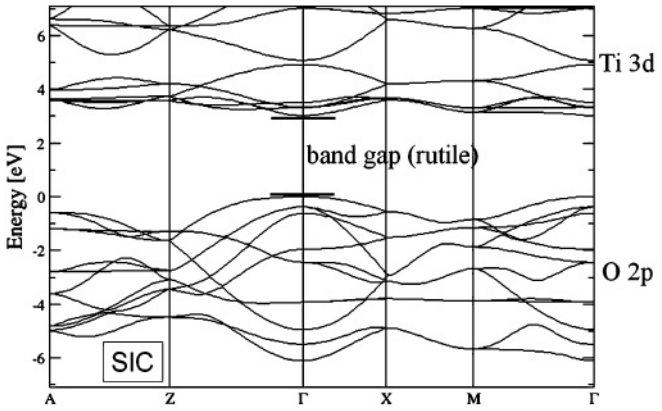

FIG. 6. Band structure of bulk TiO_2 (rutile structure) calculated with modified SIC-PP. The VBM is set to 0 eV. Again each group of bands is labeled according to the dominant orbitals involved. The SIC-LDA band gap is 3.02 eV.

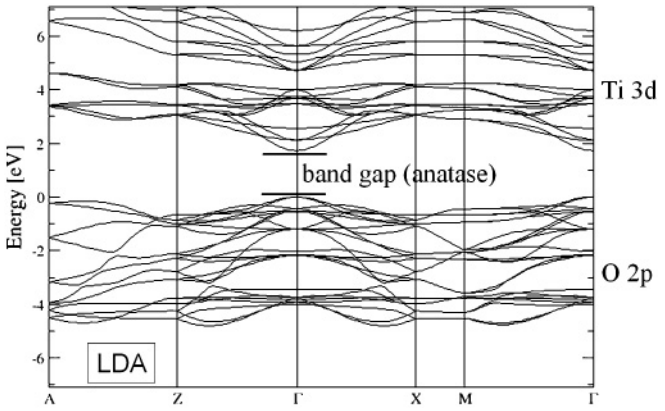

FIG. 7. Band structure of bulk TiO_2 (anatase structure) calculated in LDA. The VBM is set to 0 eV. We find a LDA band gap of 1.73 eV. The primary orbital character for each group of bands is indicated on the right side.

was 3.46 eV which both deviate less than 10 percent from the experimental values. However, we decided to continue our calculations with the individually adjusted PPs since a precise description of the undoped band structures is the best starting point for the determination of the defect levels of the dopants, and because the solid-state adjustment of the ASIC in the crystal structures may be slightly different.

E. Electronic defect levels at GB in pure TiO_2

In Figs. 9 and 10 sections of the total electronic densities of states (DOS) for the six undoped GBs and the respective perfect rutile or anatase crystal calculated with SIC-LDA are depicted. $GB3_r$ as well as all the anatase GBs show deep levels in the band gap. These deep levels are not an artifact of the SIC-PPs since they already appear in LDA. However in LDA the levels lie closer to the band edges. In our previous study of GBs in ZnO,[16] we have only found deep levels above the VBM. For TiO_2 $GB3_r$, $GB5_a$, and $GB6_a$ also have deep levels below the conduction-band minimum (CBM). An analysis of the DOS of the individual atoms revealed that the deep levels below the CBM originate from under-coordinated Ti atoms

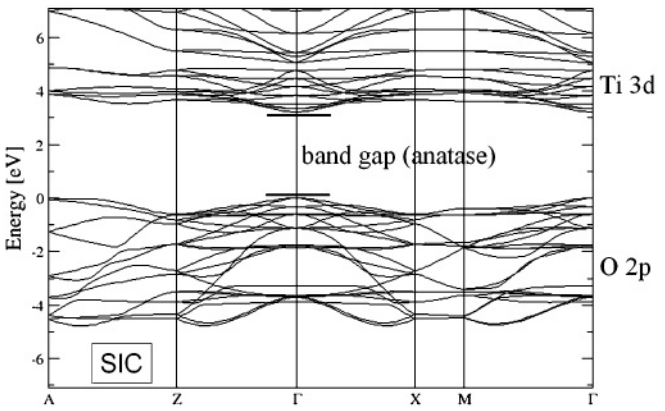

FIG. 8. Band structure of bulk TiO_2 (anatase structure) calculated with modified SIC-PP. The VBM is set to 0 eV. Again each group of bands is labeled according to the dominant orbitals involved. The SIC-LDA band gap is 3.22 eV.

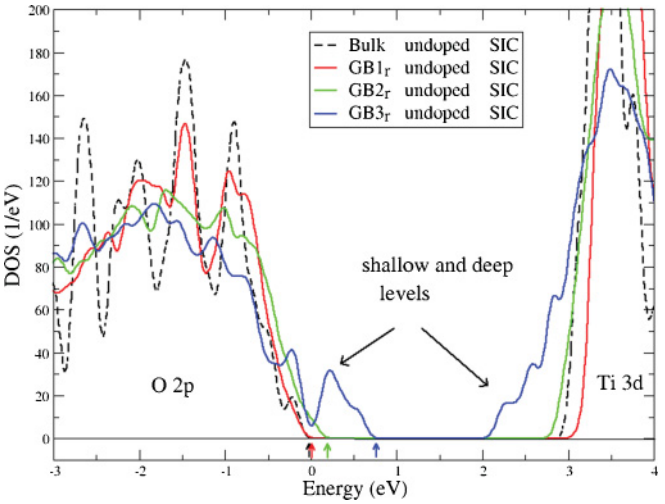

FIG. 9. (Color online) Comparison of the total densities of states of the three rutile GBs and the perfect TiO_2 rutile single crystal calculated with the SIC scheme. The small colored arrows below the zero line indicate the occupation level for each supercell. $GB3_r$ shows deep levels due to under-coordinated O and Ti atoms.

(with only 5 instead of 6 O neighbors) and the deep levels above the VBM from under-coordinated O atoms (oxygen dangling bonds, with 2 instead of 3 Ti neighbors). However, O atoms with dangling bonds do not necessarily lead to deep levels. Performing similar calculations Dawson *et al.*[22] investigated the undoped (210)[001] Σ5 GB (our $GB2_r$ shown in Fig. 3). Their calculated DOS in LDA showed only shallow levels mainly associated with the upper edge of the valence band. This is in perfect agreement with our LDA (not shown) and also SIC-LDA results (see Fig. 9). Thus our conclusion is that under-coordinated O atoms in TiO_2 can produce deep levels but do not have to. Deep levels due to under-coordinated O

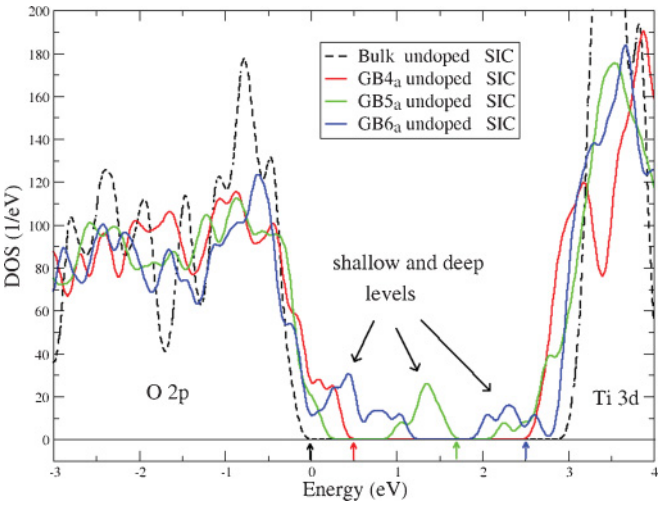

FIG. 10. (Color online) Comparison of the total densities of states for the three anatase GBs and the perfect TiO_2 anatase single crystal calculated with the SIC-PP scheme. The small colored arrows below the zero line indicate the occupation level for each supercell. Especially $GB5_a$ has deep electronic levels in the middle of the gap which originate from two dangling oxygen bonds per supercell unit.

atoms do also require certain geometric arrangements of the environment.

1. Oxygen vacancy and titanium interstitial

Before we discuss the extrinsic dopants we briefly comment on the oxygen vacancy and the titanium interstitial embedded in the prefect rutile or anatase single crystal which are seen as the key reason for the intrinsic *n* conductivity of TiO_2.[13,46,47] Since for all the defects our findings differed very little for the rutile and anatase structures we show either the DOS results of rutile or anatase in order to limit the number of figures.

According to the analysis of the defect formation energy the V_O^0 and V_O^{2+} are the preferred charge states of the oxygen vacancy. In Fig. 11 the DOS for these charge states are plotted in LDA and in SIC-LDA. There are no donor levels visible below the CBM which is in accordance with two other DFT studies.[11,13]

The titanium interstitial prefers the Ti_i^{4+} state. Its DOS are depicted in Fig. 12. In LDA one observes an energy level 0.25 eV below the CBM which is also reported by Ref. 11. These authors discuss the unphysical self-interactions contained in LDA and suspect that their level is linked to the blue coloration of undoped reduced TiO_2 reported by Cronemeyer[46] which is associated with levels 0.75 eV below the CBM. Our SIC results for the Ti_i^{4+} confirm their prediction and thus give strong evidence for the blue coloration. Also Ref. 7, in which LDA+U was used, predicts a level at 0.7 eV below the CBM.

Since the Ti_i provides shallow donor states combined with moderate formation energies in the *n* conducting regime, the Ti_i may cause the intrinsic *n* conductivity.

F. Electronic defect levels at GB in doped TiO_2

As discussed for ZnO in Ref. 16 there is no obvious bulk SIC reference for extrinsic dopants. For N, Al, Ga, and Nb in TiO_2 one can choose as a physical guideline the weight factors

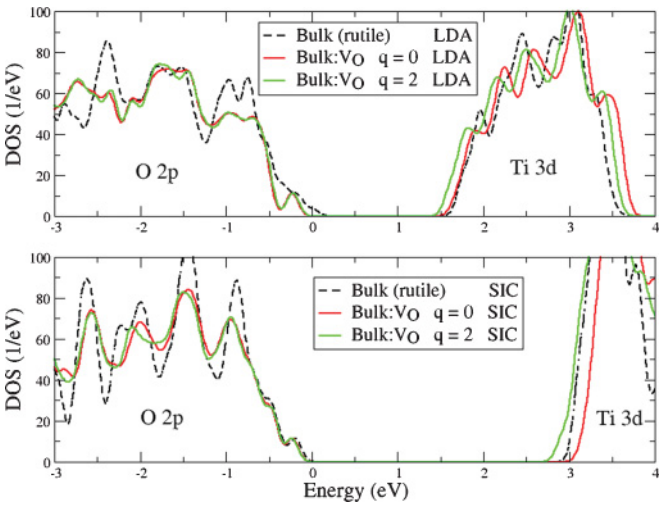

FIG. 11. (Color online) The total densities of states of the bulk TiO_2 rutile crystal with an oxygen vacancy determined in LDA and with SIC-PP. The oxygen vacancy leads to minor corrections of the band edges and does not produce shallow donor levels below the CBM.

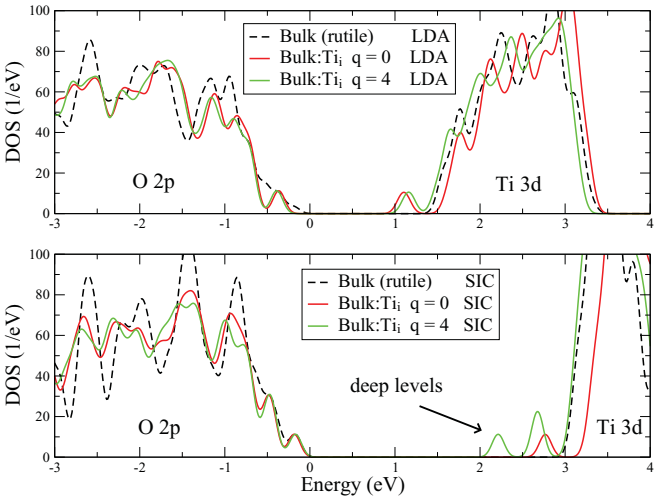

FIG. 12. (Color online) The total densities of states of the bulk TiO_2 rutile crystal with a titanium interstitial determined in LDA and with SIC-PP. The deep levels at 0.75 eV below the CBM may be the reason for the blue coloration observed by Cronemeyer (Ref. 46).

w_l according to the atoms they substitute (see Table I) since the occupation varies rather weakly. For nitrogen for example we have chosen $w_1 = 0.8$ or 0.9 as for oxygen depending on whether it was put into TiO_2 with rutile or anatase structure. In the case of Ga the 3*d* shell is fully occupied and thus requires a SIC of 100% which is reflected by the choice of $w_2 = 1$ (see Table I).

1. n-type dopant Nb *in* TiO_2

In Fig. 13 we show the DOS of the $GB2_r$ and the bulk crystal in rutile structure doped with Nb on Ti sites. The Nb_{Ti}^+ defect (lowest in energy according to Fig. 4) creates shallow donor levels below the CBM. At the $GB2_r$ these levels are more spread out and the interaction of the dopant with the GB leads to additional deep levels. We observed these two features as well for the other investigated GBs. For high Nb concentrations at the GBs we thus predict a lowering of the optical transparency due to Nb-caused defect levels. However, the combination of low defect formation energies and shallow donor levels makes Nb a promising candidate for the production of highly *n*-conducting TiO_2. This is in line with recent experiments by Sato *et al.* (Ref. 48 and references therein).

2. p-type dopants N, Al, *and* Ga *in* TiO_2

In order to be good candidates for *p* doping N, Al, and Ga should generate shallow acceptor levels above the VBM. The N_O^- defect fulfills that condition in the bulk and at the $GB2_r$ which can be seen in Fig. 14. Unfortunately nitrogen shows an amphoteric behavior turning into a donor at low electron chemical potential μ_e (see Fig. 4). According to Fig. 14 the N_O^+ defects do not provide donor levels if they are situated in the bulk, but at $GB2_r$ (and similarly at the other considered GBs) shallow donor levels at the CBM are formed. These N_O^+ defects would then inhibit an effective *p* doping of TiO_2. Concerning the optical transparency we predict a reduction due to N doping. The deep levels within the band gap also reported

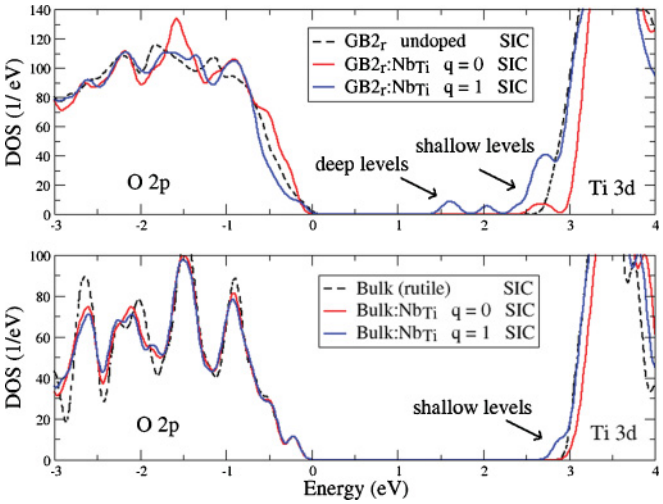

FIG. 13. (Color online) The total densities of states of the Nb-doped $GB2_r$ and the bulk TiO_2 rutile crystal calculated with the SIC-PP scheme. The Nb_{Ti}^{+} defects generate shallow donor levels and create additionally some deeper levels at $GB2_r$ which can reduce the optical transparency.

by Ref. 8 at about the same positions can cause a decrease in the photothreshold energy of TiO_2 (see also the review by Thompson and Jates[49] for a discussion of the theoretical and experimental findings).

Al and Ga in TiO_2 can be treated together since our analysis showed that their formation energies as well as their electronic defect levels are very similar. According to Fig. 4 Al and Ga have mainly the same amphoteric behavior as N. Again in the bulk the behavior is promising since the Al_{Ti}^{-} and Ga_{Ti}^{-} defects generate shallow acceptor defects whereas the donor Al_{Ti}^{+} and Ga_{Ti}^{+} defects do not produce relevant levels. At GBs however, as in the case of nitrogen, we find donor states which are relevant for low values of the electron chemical potential μ_e.

According to the formation energy analysis Al and Ga prefer the neutral defect state for the *n*-conducting regime

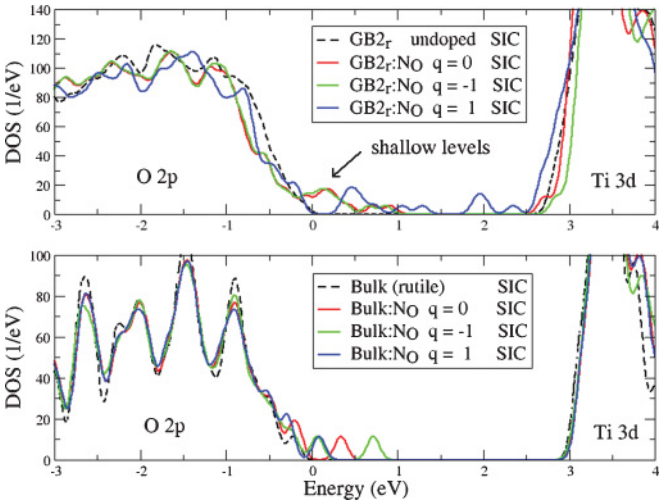

FIG. 14. (Color online) The total densities of states of the N-doped $GB2_r$ and the bulk TiO_2 rutile crystal calculated with SIC-PP scheme. Nitrogen doping leads to shallow donor or acceptor levels depending on the considered N_O^{+} or N_O^{-} defect.

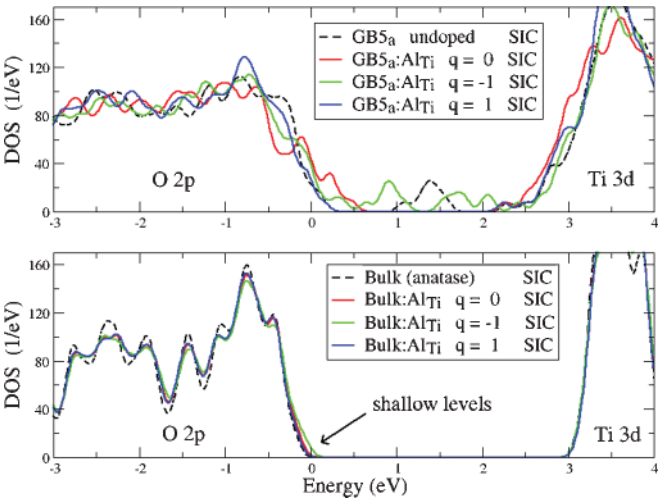

FIG. 15. (Color online) The total densities of states of the Al-doped $GB5_a$ and the bulk TiO_2 anatase crystal calculated with SIC-PP scheme. The Al_{Ti}^{-1} defect generates shallow acceptor levels in the bulk. However, according to Fig. 4 Al_{Ti}^{+1} is the preferred defect state for the *p* regime which does not provide shallow levels close to VBM. Interestingly, it opens the band gap at $GB5_a$.

at $GB5_a$ (see Fig. 4). According to Fig. 15 the configuration $GB5_a$:Al_{Ti}^{0} makes all the deep levels in the middle of the gap disappear which means that $GB5_a$ is more transparent than in the undoped state (see Fig. 10).

Especially for Al-doped TiO_2, we find a general absence of deep levels for all our investigated systems. This is in accordance with the experimental finding of Ref. 50 that TiO_2:Al is colorless. However, the theoretical work of Islam *et al.* using a DFT-HF hybrid method[52] reports that the isolated Al_{Ti}^{0} defect generates a deep level in the band gap. According to their study Al in a substitutional site in combination with an oxygen vacancy does not introduce any deep defect level in the band gap. Since we focused in this study on GBs and did not consider the defect complex Al_{Ti}-V_O we cannot further comment on this discrepancy.

Ga doping reduced the number of deep levels in most cases. However, the effect we observed was weaker than in the case of Al. For example at $GB3_a$ Ga created deep levels which Al did not.

IV. SUMMARY AND CONCLUSIONS

In summary, we studied four substitutional dopants Nb, N, Al, and Ga at six different grain boundaries and in the bulk single crystals of TiO_2 with rutile or anatase structures. We found that

(1) There is a general trend of segregation to the GBs for all dopants.

(2) The defect formation energies for the dopants at the grain boundaries can differ by several eV from the perfect crystal values which can be rationalized by the different local environments at the GBs compared to the perfect bulk. These different environments can lead to deviating preferred charge states for the defects at the GBs. For example pairs of under-coordinated oxygen atoms near a dopant lead to modified charged states (see $GB5_a$ in Fig. 4). Single under-coordinated

oxygen or titanium atoms did not affect the preferred charge states of adjacent defects compared to the bulk.

(3) All dopants create modified defect levels near grain boundaries. They tend to be spread out and also their positions can change.

(4) The position of the additional deep levels at 0.75 eV below the CBM generated by a titanium interstitial (for TiO_2 with rutile structure) as found by SIC-PP can explain the blue coloration observed by Cronemeyer[46] (see Fig. 12).

(5) Doping of TiO_2 with Nb in order to obtain an *n*-conducting TCO should work since Nb defects prefer the Nb_{Ti}^{+} donor charge state which can serve as a single donor because it produces shallow levels below the CBM (see Fig. 13).

(6) Doping of TiO_2 with N, Al, and Ga in order to obtain a *p*-conducting TCO is not very promising according to our findings since these dopants show amphoteric behavior and turn into donors for low values of the electron chemical potential. The generation of levels within the band gap due to N doping may cause a decrease in the photothreshold energy for TiO_2. Ga doping does merely create deep levels whereas Al doping even reduces deep levels and should lead to an improved transparency of polycrystalline samples.

ACKNOWLEDGMENTS

Financial support for this work was provided by the Fraunhofer-Gesellschaft in Germany (MAVO project METCO) and by the European Commission through Contract No. NMP3-LA-2010-246334 (ORAMA). We thank B. Szyszka and P. Loebmann for valuable discussions and helpful comments.

*wolfgang.koerner@iwm.fraunhofer.de

[1] K. M. Glassford and J. R. Chelikowsky, Phys. Rev. B **46**, 1284 (1992).
[2] K. Watanabe, K. Inoue, and F. Minami, Phys. Rev. B **46**, 2024 (1992).
[3] H. Tang, H. Berger, P. E. Schmidt, and F. Levy, Solid State Commun. **87**, 847 (1993).
[4] T. L. Thompson and J. T. Yates Jr., Chem. Rev. **106**, 4428 (2006).
[5] R. Asahi, T. Morikawa, T. Ohwaki, K. Aoki, and Y. Taga, Science **293**, 269 (2001).
[6] K. Yang, Y. Dai, and B. Huang, J. Phys. Chem. C **111**, 18985 (2007).
[7] J. Osorio-Guillen, S. Lany, and A. Zunger, Phys. Rev. Lett. **100**, 036601 (2008).
[8] C. di Valentin, E. Finazzi, G. Pacchioni, A. Selloni, S. Livraghi, M. C. Paganini, and E. Giamello, Chem. Phys. **339**, 44 (2007).
[9] R. N. Blumenthal, J. Coburn, J. Baukus, and W. M. Hirthe, J. Phys. Chem. Solids **26**, 643 (1966).
[10] J. He and S. B. Sinnott, J. Am. Ceram. Soc. **88**, 737 (2005).
[11] E. Cho, S. Han, H.-S. Ahn, K.-R. Lee, S. K. Kim, and C. S. Hwang, Phys. Rev. B **73**, 193202 (2006).
[12] J. He, R. K. Behera, M. W. Finnis, X. Li, E. C. Dickey, S. R. Phillpot, and S. B. Sinnott, Acta Mater. **55**, 4325 (2007).
[13] S. Na-Phattalung, M. F. Smith, K. Kim, M.-H. Du, S.-H. Wei, S. B. Zhang, and S. Limpijumnong, Phys. Rev. B **73**, 125205 (2006).
[14] J. Yu, X. Zhao, and Q. Zhao, J. Mater. Sci. Lett. **19**, 1015 (2000).
[15] N. Yamada, T. Hitosugi, N. L. H. Hoang, Y. Furubayashi, Y. Hirose, S. Konuma, T. Shimada, and T. Hasegawa, Thin Solid Films **516**, 5754 (2008).
[16] W. Körner and C. Elsässer, Phys. Rev. B **81**, 085324 (2010).
[17] D. J. Wallis, N. D. Browning, P. D. Nellist, S. J. Pennycook, I. Majid, Y. Liu, and J. B. Vander Sande, J. Am. Ceram. Soc. **80**, 499 (1997).
[18] U. Dahmen, S. Paciornik, I. G. Sorzano, and J. B. Vander Sande, Interface Sci. **2**, 125 (1994).
[19] U. Dahmen, S. Paciornik, I. G. Sorzano, and J. B. Vander Sande, Mater. Res. Soc. Symp. Proc. **357**, 127 (1995).
[20] B. Pourmellec, P. J. Durham, and G. Y. Guo, J. Phys. Condens. Matter **3**, 8195 (1991).
[21] F. M. F. de Groot, J. Faber, J. J. M. Michiels, M. T. Czyzyk, M. Abbate, and J. C. Fuggle, Phys. Rev. B **48**, 2074 (1993).
[22] I. Dawson, P. D. Bristowe, M.-H. Lee, M. C. Payne, M. D. Segall, and J. A. White, Phys. Rev. B **54**, 13727 (1996).
[23] R. Asahi, Y. Taga, W. Mannstadt, and A. J. Freeman, Phys. Rev. B **61**, 7459 (2000).
[24] R. Janisch and N. A. Spaldin, Phys. Rev. B **73**, 035201 (2006).
[25] J. P. Perdew and A. Zunger, Phys. Rev. B **23**, 5048 (1981).
[26] D. Vogel, P. Krüger, and J. Pollmann, Phys. Rev. B **54**, 5495 (1996).
[27] C. Elsässer, N. Takeuchi, K. M. Ho, C. T. Chan, P. Braun, and M. Fähnle, J. Phys. Condens. Matter **2**, 4371 (1990).
[28] K. M. Ho, C. Elsässer, C. T. Chan, and M. Fähnle, J. Phys. Condens. Matter **4**, 5189 (1992).
[29] B. Meyer, K. Hummler, C. Elsässer, and M. Fähnle, J. Phys. Condens. Matter **7**, 9201 (1995).
[30] F. Lechermann, M. Fähnle, B. Meyer, and C. Elsässer, Phys. Rev. B **69**, 165116 (2004).
[31] D. Vanderbilt, Phys. Rev. B **32**, 8412 (1985).
[32] C. D. Pemmaraju, T. Archer, D. Sanchez-Portal, and S. Sanvito, Phys. Rev. B **75**, 045101 (2007).
[33] A. P. Sutton and R. W. Balluffi, *Interfaces in Crystalline Materials* (Oxford Universtiy Press, Oxford, 1995).
[34] W. H. Press, B. P. Flannery, S. A. Teukolsky, and W. T. Vettering, *Numerical Recipies* (Cambridge University Press, Cambridge, 1986), Chap. 10.7.
[35] C. G. Van de Walle and J. Neugebauer, J. Appl. Phys. **95**, 3851 (2003).
[36] Y. Yan, S. B. Zhang, and S. T. Pantelides, Phys. Rev. Lett. **86**, 5723 (2001).
[37] P. Deak, B. Aradi, T. Frauenheim, and A. Gali, Mater. Sci. Eng. B **154-155**, 187 (2008).
[38] W. Körner and C. Elsässer, Phys. Rev. B **83**, 205306 (2011).
[39] J. M. Carlsson, H. S. Domingos, P. D. Bristowe, and B. Hellsing, Phys. Rev. Lett. **91**, 165506 (2003).
[40] C. J. Howard, T. M. Sabine, and F. Dickson, Acta Crystallogr. Sect. B **47**, 462 (1991).
[41] J. D. Cox, D. D. Wagman, and V. A. Medvedev, *CODATA Key Values for Thermodynamics* (Hemisphere Publishing Corp., New York, 1984).

[42] A. Janotti, J. B. Varley, P. Rinke, N. Umezawa, G. Kresse, and C. G. Van de Walle, Phys. Rev. B **81**, 085212 (2010).
[43] S.-G. Park, B. Magyari-Köpe, and Y. Nishi, Phys. Rev. B **82**, 115109 (2010).
[44] S. P. Kowalczyk, F. R. McFeely, L. Ley, V. T. Gritsyna, and D. A. Shirley, Solid State Commun. **23**, 161 (1977).
[45] R. Sanjinés, H. Tang, H. Berger, F. Gozzo, G. Margaritondo, and F. Lévy, J. Appl. Phys. **75**, 2945 (1994).
[46] D. C. Cronemeyer, Phys. Rev. **113**, 1222 (1959).
[47] X. Hoshino, N. L. Peterson, and C. L. Wiley, J. Phys. Chem. Solids **46**, 1397 (1985).
[48] Y. Sato, H. Akizuki, T. Kamiyama, and Y. Shigesato, Thin Solid Films **516**, 5758 (2008).
[49] T. L. Thompson and J. T. Jates Jr., Chem. Rev. **106**, 4428 (2006).
[50] U. Gesenhues, J. Photochem. Photobiol. A **139**, 243 (2001).
[51] M. M. Islam, T. Bredow, and A. R. Gerson, Phys. Rev. B **76**, 045217 (2007).
[52] T. Bredow and A. R. Gerson, Phys. Rev. B **61**, 5194 (2000).